LANGLEY GRANT

IN-32

84127

ELECTROMAGNETIC SCATTERING BY IMPEDANCE STRUCTURES

p.36

Semiannual Report

Constantine A. Balanis and Timothy Griesser
February 1, 1987 - July 31, 1987

Department of Electrical and Computer Engineering
Arizona State University
Tempe, AZ 85287

Grant No. NAG-1-562
National Aeronautics and Space Administration
Langley Research Center
Hampton, VA 23665

ABSTRACT

The scattering of electromagnetic waves from impedance structures is investigated, and current work on antenna pattern calculation is presented. A general algorithm for determining radiation patterns from antennas mounted near or on polygonal plates is presented. These plates are assumed to be of a material which satisfies the Leontovich (or surface impedance) boundary condition. Calculated patterns including reflection and diffraction terms are presented for numerous geometries, and refinements are included for antennas mounted directly on impedance surfaces. For the case of a monopole mounted on a surface impedance ground plane, computed patterns are compared with experimental measurements. This work in antenna pattern prediction forms the basis of understanding of the complex scattering mechanisms from impedance surfaces. It provides the foundation for the analysis of backscattering patterns which, in general, are more problematic than calculation of antenna patterns. Further proposed study of related topics, including surface waves, corner diffractions, and multiple diffractions, is outlined.

I. INTRODUCTION

During the semiannual period beginning February 1, 1987 and ending July 31, 1987, research on scattering from impedance structures has progressed under funding through Grant No. NAG-1-562 entitled "Electromagnetic Backscattering by Corner Reflectors". The research during this period concentrated on scattering from impedance surfaces and edges using extensions of the Uniform Theory of Diffraction (UTD). An impedance surface is a common and useful approximation to a lossy material or a dielectric coated conductor. A large portion of the research involved antenna pattern prediction for antennas mounted on or near impedance surfaces. This work will provide the foundation for understanding backscattering from lossy or dielectric coated bodies which can be represented by the Leontovich surface impedance boundary condition. Historically, in perfectly conducting UTD analyses, the antenna pattern analysis is approached first since it is generally less problematic than the backscattering analysis. Similarly in this imperfect conductor theory, it is expected that full understanding of the scattering mechanisms (including reflection, edge diffractions, surface waves and perhaps corner diffraction) can be derived from the antenna prediction problem, and such techniques will be amenable to the imperfect conductor backscatter problem.

In addition to the progress in the current research, the publication of past research is being pursued. Two papers related to research funded under this grant have been accepted during this reporting period for publication in a leading journal. The first,

entitled "Backscatter Analysis of Dihedral Corner Reflectors using the Physical Theory of Diffraction", is currently scheduled for publication in the September 1987 issue of the IEEE Transactions on Antennas and Propagation. The second, entitled "Dihedral Corner Reflector Backscatter using Higher-Order Reflections and Diffractions", is scheduled for publication in the November 1987 issue of the same journal. Both these papers are coauthored by T. Griesser and C. A. Balanis. The first is a PTD analysis and the second is a uniform GTD analysis of backscattering from a corner reflector. These papers represent major results from research funded under this grant and presented in earlier progress reports.

In addition a paper entitled "Diffractions from a lossy polygonal plate in the presence of an antenna" was presented and published at the IEEE APS/URSI Joint International Symposium in Blacksburg, VA during June 15-19, 1987. This conference paper presented results of research conducted during this and a portion of the preceding semiannual progress report.

The current research utilizes the Uniform Geometrical Theory of Diffraction (UTD) for an imperfectly conducting ground plane, presented by Volakis [1] in 1986. This theory made available UTD coefficients for a half-plane for both normal and oblique incidence, and these coefficients revert to the perfectly conducting case [2] as the normalized surface impedance, η, vanishes. The diffraction coefficients are written in the form of a 2×2 matrix which defines a dyadic diffraction coefficient consisting of four nonzero dyads. The coefficients are formulated by the UTD ansatz from Senior's Wiener-Hopf

solution [3] for oblique incidence on a half-plane and are calculated in terms of the Maliuzhinets [4] Ψ_π function. The Ψ_π function has been suitably approximated by Volakis and Senior [5].

For completeness, the theory of imperfect conducting wedge diffraction needs to be extended to wedges of arbitrarily angle, to include corner diffraction mechanisms, to add extended spectral theory contributions for near grazing incidence, and to include surface wave effects. However the half-plane theory by itself can provide useful solutions to many classical problems involving structures composed of flat, imperfectly conducting plates.

The problem which is studied here is that of radiation pattern prediction for an arbitrary antenna in the presence of an imperfectly conducting polygonal plate. The polygonal plate might be a first-order approximation to an actual structure the antenna is mounted on. The problem is fully specified by the antenna frequency, pattern, polarization, location, and orientation and the plate shape, size, orientation, and surface impedance. For any given observation point, the total field is calculated as the sum of direct and reflected fields, as well as one diffracted field per edge of the polygonal plate.

If double diffraction between edges is included, then one double diffraction per pair of edges is needed, and if the polygonal plate has N edges, then N(N-1) double diffractions are possible. However if the double diffraction is calculated in the classical way, that is, by multiplying the field diffracted from one edge by the diffraction coefficient at the next edge, the theory predicts zero fields. This occurs because the UTD coefficients are zero when the observation point

is on the surface for either polarization and for any surface impedance except for the single special case of hard polarization and zero surface impedance; i.e., for the perfectly conducting hard polarization case.

To calculate nonzero double diffraction fields, the extended spectral theory of diffraction [6] is required. In this theory, the diffracted field is represented as a sum (or integral) of slowly varying inhomogeneous waves, each of which is multiplied by a diffraction coefficient at the diffracting edge. In this theory, the observation angles of these inhomogeneous waves are, in general, complex numbers, each consisting of a real angle (near the actual geometrical angle) and an imaginary angle. The diffraction coefficients, analytically continued into the complex plane, are then nonzero whenever the observation point lies on the surface. Hence it is possible to determine nonzero double diffraction terms as a sum (or integral) of these diffracted inhomogeneous waves.

If the source is located on the surface of the plate, a similar problem is encountered. The diffraction coefficients at the edges are all zero and do not contribute to the total field leading to large discontinuities in the plane of the plate. This problem can be overcome by reevaluating the asymptotic UTD solution [7], [8]. The UTD solution [1], which predicts vanishing diffraction coefficients for grazing incidence, retains only the first term of an aymptotic expansion. By retaining the higher order nonzero term [7] the diffraction coefficients correctly compensate for the pattern discontinuities. Comparisons of this technique with experimental measurements are presented in this report.

II. SCATTERING FROM POLYGONAL IMPEDANCE PLATES

A. Geometry

The goal of this work is to analyze the scattering pattern of an arbitrary antenna in the presence of an arbitrary polygonal plate. The formulation should be readily incorporated into a computer program and should produce computed patterns in arbitrary planes given the minimum physical information. This information, in this case, is the antenna frequency, pattern, polarization, location, and orientation and the location of the polygonal plate vertices, as well as the surface impedance of the plate. The geometrical formulation is based on earlier work by Burnside [9] for the perfectly conducting plate case, and modifications are added to make the solution more general as well as to allow the analysis of imperfect conductors of relative surface impedance η.

If an origin is chosen at some arbitrary reference point, then the source position is defined by the position vector $\bar{s}$ and the scattering direction is defined by a unit direction vector $\hat{a}_r$. In the scattering direction (θ,ϕ) the spherical unit vectors are

$$\hat{a}_r = \sin\theta\cos\phi\ \hat{a}_x + \sin\theta\sin\phi\ \hat{a}_y + \cos\theta\ \hat{a}_z \tag{1a}$$

$$\hat{a}_\theta = \cos\theta\cos\phi\ \hat{a}_x + \cos\theta\sin\phi\ \hat{a}_y - \sin\theta\ \hat{a}_z \tag{1b}$$

$$\hat{a}_\phi = -\sin\phi\ \hat{a}_x + \cos\phi\ \hat{a}_y \tag{1c}$$

The far-field radiation pattern of the source is written as

$$\vec{E}_s(r,\theta,\phi) = \vec{E}_s(\theta,\phi)\,\frac{e^{-jkr}}{r} = \left[\hat{a}_\theta E_\theta(\theta,\phi) + \hat{a}_\phi E_\phi(\theta,\phi)\right]\frac{e^{-jkr}}{r} \qquad (2)$$

where r is the distance to an observation point and $\vec{E}_s(\theta,\phi)$ is the far-field pattern.

The polygonal plate is identified by defining a position vector $\vec{v}_m$ to each vertex, where $1 \le m \le N$, for the N vertices. The ordering is chosen such that m increases in a counterclockwise direction when viewed from the source. Unit edge vectors $\hat{e}_m$ are defined by

$$\hat{e}_m = (\vec{v}_{m+1} - \vec{v}_m)/|\vec{v}_{m+1} - \vec{v}_m| \qquad (3)$$

where vector subscripts less than zero or greater than N are understood to be evaluated modulo N throughout this paper. A normal unit vector to the plate in the direction of the source is

$$\hat{n} = (\hat{e}_{m-1} \times \hat{e}_m)/|\hat{e}_{m-1} \times \hat{e}_m| \qquad (4)$$

where vertex m has an included angle less than π. A unit vector $\hat{e}'_m$ in the plane of the plate, perpendicular to the edge, and in the direction of the finite plate is

$$\hat{e}'_m = \hat{n} \times \hat{e}_m \qquad (5)$$

Two nonparallel unit vectors $\hat{e}_1$ and $\hat{e}_2$ are chosen as basis vectors $\hat{t}_1$ and $\hat{t}_2$ for the plane of the polygonal plate.

An $e^{j\omega t}$ time convention is assumed and suppressed throughout this report.

B. The Direct Field

The direct field from the source in the observation direction is given by

$$\bar{E}_d(\theta,\phi) = \bar{E}_s(\theta,\phi)\,\frac{e^{-jkr}}{r} \tag{6}$$

unless the observation direction is shadowed by the polygonal plate. To determine if the ray from the source is shadowed, the vector equation

$$\bar{v}_1 + \alpha_1 \hat{t}_1 + \alpha_2 \hat{t}_2 = \bar{s} + \alpha_3 \hat{a}_r \tag{7}$$

is solved. This equation uses the plate basis vectors to determine the intersection point of the ray with the plate, and it represents three scalar equations in the three unknowns α_1, α_2 and α_3. If α_3 is negative, then there is no intersection of the ray with the plate. If α_3 is positive and the point $\bar{s} + \alpha_3 \hat{a}_r$ lies within the finite plate boundaries, then there will be shadowing of the ray by the plate.

To determine if this point lies within the plate boundary, a unit vector $\hat{p}_m$ is defined for each vertex by

$$\hat{p}_m = (\bar{v}_m - \bar{s} - \alpha_3 \hat{a}_r)/|\bar{v}_m - \bar{s} - \alpha_3 \hat{a}_r| \tag{8}$$

If the sum

$$S = \left| \sum_{m=1}^{N+1} \left[\cos^{-1}(\hat{p}_m \cdot \hat{p}_{m+1}) \right] \cdot \operatorname{sgn}\left[\hat{n} \cdot (\hat{p}_m \times \hat{p}_{m+1}) \right] \right| \tag{9}$$

is equal to 2π then the point lies within the boundary and if the sum is equal to 0 then the point lies outside the polygonal boundary. In the sum, the range of the inverse cosine is chosen as $[0,\pi)$ if

$(\hat{p}_m \times \hat{p}_{m+1}) \cdot \hat{n} \geq 0$ and $(-\pi, 0)$ if $(\hat{p}_m \times \hat{p}_{m+1}) \cdot \hat{n} < 0$.

C. The Reflected Field

To determine the reflected field, the image location must be found. The source image location $\bar{s}_i$ is found by solving the vector equation

$$\bar{v}_1 + \beta_1 \hat{t}_1 + \beta_2 \hat{t}_2 = \bar{s} + \beta_3 \hat{n} \tag{10}$$

which represents three scalar equations in the three unknowns β_1, β_2, and β_3. Solving for β_3, the image location is

$$\bar{s}_i = \bar{s} + 2\beta_3 \hat{n} \tag{11}$$

With the image location known, the specular reflection point location $\bar{s}_r$ is found by

$$\bar{s}_r = \bar{v}_1 + \gamma_1 \hat{t}_1 + \gamma_2 \hat{t}_2 = \bar{s}_i + \gamma_3 \hat{a}_r \tag{12}$$

after solving the set of three scalar equations for γ_3. The reflection exists only if γ_3 is positive and the point $\bar{s}_r$ lies within the finite polygonal plate. This can be determined by the method of the previous section.

The relected field from the plate is found in terms of the incident field and the appropriate reflection coefficients for the principal polarizations. The angular direction (θ_r, ϕ_r) from the source to the reflection point is given by

$$\theta_r = \cos^{-1}\left[\frac{\vec{s}_r - \vec{s}}{|\vec{s}_r - \vec{s}|} \cdot \hat{a}_z\right] \tag{13a}$$

$$\phi_r = \tan^{-1}\left[\frac{(\vec{s}_r - \vec{s})\cdot \hat{a}_y}{(\vec{s}_r - \vec{s})\cdot \hat{a}_x}\right] \tag{13b}$$

where the value of the inverse tangent must be determined in the correct quadrant by the signs of the numerator and denominator. The spherical coordinate vectors at the reflection point are

$$\hat{a}_r^r = \sin\theta_r\cos\phi_r\hat{a}_x + \sin\theta_r\sin\phi_r\hat{a}_y + \cos\theta_r\hat{a}_z \tag{14a}$$

$$\hat{a}_\theta^r = \cos\theta_r\cos\phi_r\hat{a}_x + \cos\theta_r\sin\phi_r\hat{a}_y - \sin\theta_r\hat{a}_z \tag{14b}$$

$$\hat{a}_\phi^r = -\sin\phi_r\hat{a}_x + \cos\phi_r\hat{a}_y \tag{14c}$$

The incident and reflected soft and hard polarization unit vectors at the specular reflection point are

$$\hat{a}_s^i = \hat{a}_s^r = (\hat{n} \times \hat{a}_r^r)/|\hat{n} \times \hat{a}_r^r| \tag{15a}$$

$$\hat{a}_h^i = \hat{a}_s \times \hat{a}_r^r \qquad \hat{a}_h^s = \hat{a}_s \times \hat{a}_r \tag{15b}$$

The soft and hard reflection coefficients are

$$\Gamma_s(\Psi) = (\eta\cos\Psi - 1)/(\eta\cos\Psi + 1) \tag{16a}$$

$$\Gamma_h(\Psi) = (\cos\Psi - \eta)/(\cos\Psi + \eta) \tag{16b}$$

where Ψ is the angle of incidence given by

$$\Psi = \sin^{-1}\left|\hat{a}_r^r \times \hat{n}\right| \tag{17}$$

The field at the specular reflection point (suppressing the phase and spreading factor) is

$$\vec{E}_s(\theta_r, \phi_r) = \left[\hat{a}_\theta^r E_\theta(\theta_r, \phi_r) + \hat{a}_\phi^r E_\phi(\theta, \phi)\right] \tag{18}$$

The incident hard and soft polarization components are, respectively

$$\left[\bar{E}_s(\theta_r,\phi_r)\cdot\hat{a}_h^i\right]\hat{a}_h^i = \left[(\hat{a}_\theta^r\cdot\hat{a}_h^i)E_\theta(\theta_r,\phi_r) + (\hat{a}_\phi^r\cdot\hat{a}_h^i)E_\phi(\theta_r,\phi_r)\right]\hat{a}_h^i \quad (19)$$

$$\left[\bar{E}_s(\theta_r,\phi_r)\cdot\hat{a}_s^i\right]\hat{a}_s^i = \left[(\hat{a}_\theta^r\cdot\hat{a}_s^i)E_\theta(\theta_r,\phi_r) + (\hat{a}_\phi^r\cdot\hat{a}_s^i)E_\phi(\theta_r,\phi_r)\right]\hat{a}_s^i \quad (20)$$

while the reflected hard and soft polarization components are, respectively

$$\Gamma_h(\Psi)\left[\bar{E}_s(\theta_r,\phi_r)\cdot\hat{a}_h^i\right]\hat{a}_h^r \quad (21)$$

$$\Gamma_s(\Psi)\left[\bar{E}_s(\theta_r,\phi_r)\cdot\hat{a}_s^i\right]\hat{a}_s^r \quad (22)$$

Then the θ and ϕ components of the total reflected field are

$$\begin{aligned}\bar{E}_r(\theta,\phi) = {} & \left[(\hat{a}_\theta^r\cdot\hat{a}_h^i)E_\theta(\theta_r,\phi_r) + (\hat{a}_\phi^r\cdot\hat{a}_h^i)E_\phi(\theta_r,\phi_r)\right]\Gamma_h(\Psi)(\hat{a}_h^r\cdot\hat{a}_\theta^r) \quad (23)\\ & + \left[(\hat{a}_\theta^r\cdot\hat{a}_s^i)E_\theta(\theta_r,\phi_r) + (\hat{a}_\phi^r\cdot\hat{a}_s^i)E_\phi(\theta_r,\phi_r)\right]\Gamma_s(\Psi)(\hat{a}_s^r\cdot\hat{a}_\theta)\Big]\hat{a}_\theta\\ & + \left[(\hat{a}_\theta^r\cdot\hat{a}_h^i)E_\theta(\theta_r,\phi_r) + (\hat{a}_\phi^r\cdot\hat{a}_h^i)E_\phi(\theta_r,\phi_r)\right]\Gamma_h(\Psi)(\hat{a}_h^r\cdot\hat{a}_\phi)\\ & + \left[(\hat{a}_\theta^r\cdot\hat{a}_s^i)E_\theta(\theta_r,\phi_r) + (\hat{a}_\phi^r\cdot\hat{a}_s^i)E_\phi(\theta_r,\phi_r)\right]\Gamma_s(\Psi)(\hat{a}_s^r\cdot\hat{a}_\theta)\Big]\hat{a}_\phi\end{aligned}$$

The phase factor is reintroduced by multiplying the preceding expression by

$$\frac{1}{r}\,e^{-jk[r\,+\,\hat{a}_r\cdot(\bar{s}-\bar{s}_i)]} = e^{-jk[\hat{a}_r\cdot(\bar{s}-\bar{s}_i)]}\,\frac{e^{-jkr}}{r} \quad (24)$$

D. The Singly Diffracted Field

In determining the diffracted field associated with each edge, the diffraction point must be located on each edge, provided a diffraction point exists. The diffraction point is found using a binary search

technique described in [9] to determine the unique point on the edge where the incidence and diffraction angles are identical (satisfying the Keller cone requirement). For edge m, the endpoints are $\bar{v}_m$ and $\bar{v}_{m+1}$. A unit vector along the edge is $\hat{e}_m$. A general point on the edge is

$$\bar{v} = \bar{v}_m + t(\bar{v}_{m+1} - \bar{v}_m) \qquad 0 \leq t \leq 1 \tag{25}$$

The angle of incidence is

$$\alpha^i = \frac{\bar{v} - \bar{s}}{|\bar{v} - \bar{s}|} \cdot \hat{e}_m \tag{26}$$

and the angle of diffraction is

$$\alpha^d = \hat{a}_r \cdot \hat{e}_m \tag{27}$$

At the specular point, $\alpha^i = \alpha^d$. A binary search is used for t in the range $0 \leq t \leq 1$ to find the appropriate point $\bar{v}$ which satisfies the Keller cone requirement. If no value of t in this range is found, then the diffraction does not exist.

If a diffraction point is found, the unit vectors $\hat{a}_s$, $\hat{a}'_s$, $\hat{a}_\varphi$, $\hat{a}'_\varphi$, $\hat{a}_\beta$ and $\hat{a}'_\beta$ are defined corresponding to the ray fixed coordinate system at the point of diffraction.

$$\hat{a}'_s = (\bar{v} - \bar{s})/|\bar{v} - \bar{s}| \tag{28a}$$

$$\hat{a}_s = \hat{a}_r \tag{28b}$$

$$\hat{a}'_\varphi = (\hat{a}'_s \times \hat{e}_m)/|\hat{a}'_s \times \hat{e}_m| \tag{28c}$$

$$\hat{a}_{\varphi} = -(\hat{a}_s \times \hat{e}_m)/|\hat{a}_s \times \hat{e}_m| \tag{28d}$$

$$\hat{a}_{\beta} = \hat{a}_{\varphi}' \times \hat{a}_s' \tag{28e}$$

$$\hat{a}_{\beta}' = \hat{a}_{\varphi} \times \hat{a}_s \tag{28f}$$

and

$$\beta = \cos^{-1}(\hat{a}_s' \cdot \hat{e}_m) \tag{29a}$$

$$\varphi' = \tan^{-1}\left[\frac{-\hat{a}_s' \cdot \hat{n}}{-\hat{a}_s' \cdot \hat{e}_m}\right] \tag{29b}$$

$$\varphi = \tan^{-1}\left[\frac{\hat{a}_s \cdot \hat{n}}{\hat{a}_s \cdot \hat{e}_m}\right] \tag{29c}$$

Again, attention must be paid to the sign of the numerator and denominator of the argument of the inverse tangent function to determine the appropriate quadrant. The spherical coordinate angles at the diffraction point are

$$\theta_d = \cos^{-1}(\hat{a}_z \cdot \hat{a}_s') \tag{30a}$$

$$\phi_d = \tan^{-1}\left[\frac{\hat{a}_y \cdot \hat{a}_s'}{\hat{a}_x \cdot \hat{a}_s'}\right] \tag{30b}$$

The diffracted field is given in terms of the 2×2 matrix diffraction coefficient of Volakis by

$$\begin{bmatrix} E_{\beta}^{d} \\ E_{\varphi}^{d} \end{bmatrix} = \sqrt{s_d'}\,\frac{e^{-jks_d}}{s_d}\begin{bmatrix} D(\varphi,\varphi',\beta,\eta) & D_c(\varphi,\varphi',\beta,1/\eta) \\ -D_c(\varphi,\varphi',\beta,\eta) & D(\varphi,\varphi',\beta,1/\eta) \end{bmatrix}\begin{bmatrix} E_{\beta}^{i}(Q_E) \\ E_{\varphi}^{i}(Q_E) \end{bmatrix} \tag{31}$$

where

$$\begin{bmatrix} E_\beta^i(Q_E) \\ E_\varphi^i(Q_E) \end{bmatrix} = \begin{bmatrix} E_\theta(\theta_d,\phi_d)(\hat{a}_\theta\cdot\hat{a}_\beta') + E_\phi(\theta_d,\phi_d)(\hat{a}_\phi\cdot\hat{a}_\beta') \\ E_\theta(\theta_d,\phi_d)(\hat{a}_\theta\cdot\hat{a}_\varphi') + E_\phi(\theta_d,\phi_d)(\hat{a}_\phi\cdot\hat{a}_\varphi') \end{bmatrix} \tag{32}$$

and the diffracted field is written in terms of its β and φ components by

$$E_{diff}(\theta,\phi) = \left[E_\beta^d(\hat{a}_\beta\cdot\hat{a}_\theta) + E_\psi^d(\hat{a}_\varphi\cdot\hat{a}_\theta)\right]\hat{a}_\theta + \left[E_\beta^d(\hat{a}_\beta\cdot\hat{a}_\phi) + E_\psi^d(\hat{a}_\varphi\cdot\hat{a}_\phi)\right]\hat{a}_\phi \tag{33}$$

Also the phase and spreading factor are

$$\frac{e^{-jks_d}}{s_d} \simeq \frac{e^{-jkr}}{r}\, e^{-jk[\hat{a}_r\cdot(\bar{s}-\bar{v})]} \tag{34}$$

and $$s_d' = |\bar{s} - \bar{v}| \tag{35}$$

III. HIGHER ORDER MECHANISMS

The formulation of the preceding section is adequate when higher order diffractions, corner diffractions and surface waves are negligible. In addition, the source must not be too close to the surface of the polygonal plate. When the source antenna is very close to the polygonal plate, the diffraction mechanisms of the UTD of [1] vanish and provide no contribution to the antenna pattern. This limitation has been overcome by Tiberio [7] for the normal incidence case.

For an antenna on the surface of a imperfect conductor, the reflection coefficient at grazing incidence is -1 for both the soft and hard polarizations. Hence the geometrical optics field incident on the

diffracting edge is zero for both soft and hard polarizations. In addition, the diffraction coefficients for either polarization are zero for the grazing incidence case since the diffraction coefficients $K(\phi,\phi';\beta_0,\eta)$ of [1, eq. (4)] are based on the $K_+(\phi,\beta_0,\eta)$ split function of the Wiener-Hopf solution and the $K_+(\phi,\beta_0,\eta)$ is zero at grazing (ϕ=0) [1, eq. (11), Fig. 3]. Hence there can be no diffraction mechanism by this technique for an antenna mounted on a imperfect conductor. Indeed the solution does not reduce uniformly to the perfectly conducting case as η approaches zero for the hard polarization. The imperfect conductor hard polarization has zero diffraction for $\eta>0$ but the hard polarization perfect conductor case (η=0) can have nonzero diffractions.

This practical limitation is demonstrated with the geometry of Fig. 1 in which the problem of a quarter wave monopole on a finite ground plane is considered. The width of the strip w is 4.064 λ, the conductivity σ is 10^4 S/m, the dielectric constant ε_r is 3, and the frequency f is 1 GHz. These parameters correspond to a highly conducting surface impedance η=0.00167 (1+j). To analyze the quarter wave monopole pattern, the monopole is subdivided into small segments which can be approximated by infinitesimal current elements. Each element has a current proportional to the actual current distribution on the monopole. The problem then is reduced to a summation of field components due to infinitesimal elements above a finite ground plane at heights of up to $\lambda/4$.

The patterns of current elements above a finite ground plane, as a function of height h, are shown in Fig. 2. It is evident from Fig. 2

λ/4 MONOPOLE ON A COMPOSITE GROUND PLANE

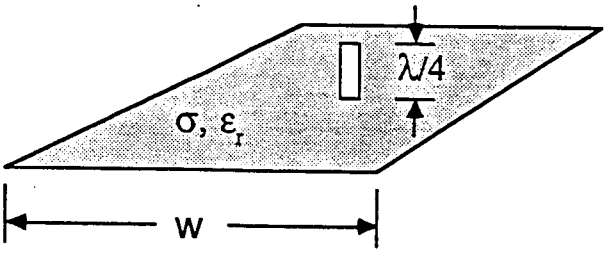

Graphite material

$$\sigma = 10^4 \text{ S/m}$$

$$\varepsilon_r = \varepsilon'/\varepsilon_0 = 3$$

$$f = \frac{\omega}{2\pi} = 1 \text{ GHz}$$

$$w = 1.22 \text{ m} = 4.064\,\lambda$$

$$\eta = \frac{1}{\eta_0}\sqrt{\frac{j\,\omega\mu}{\sigma + j\,\omega\varepsilon}}$$

$$= 0.001668(1. + j)$$

Fig. 1. Geometry and parameters for a monopole mounted on a composite ground plane.

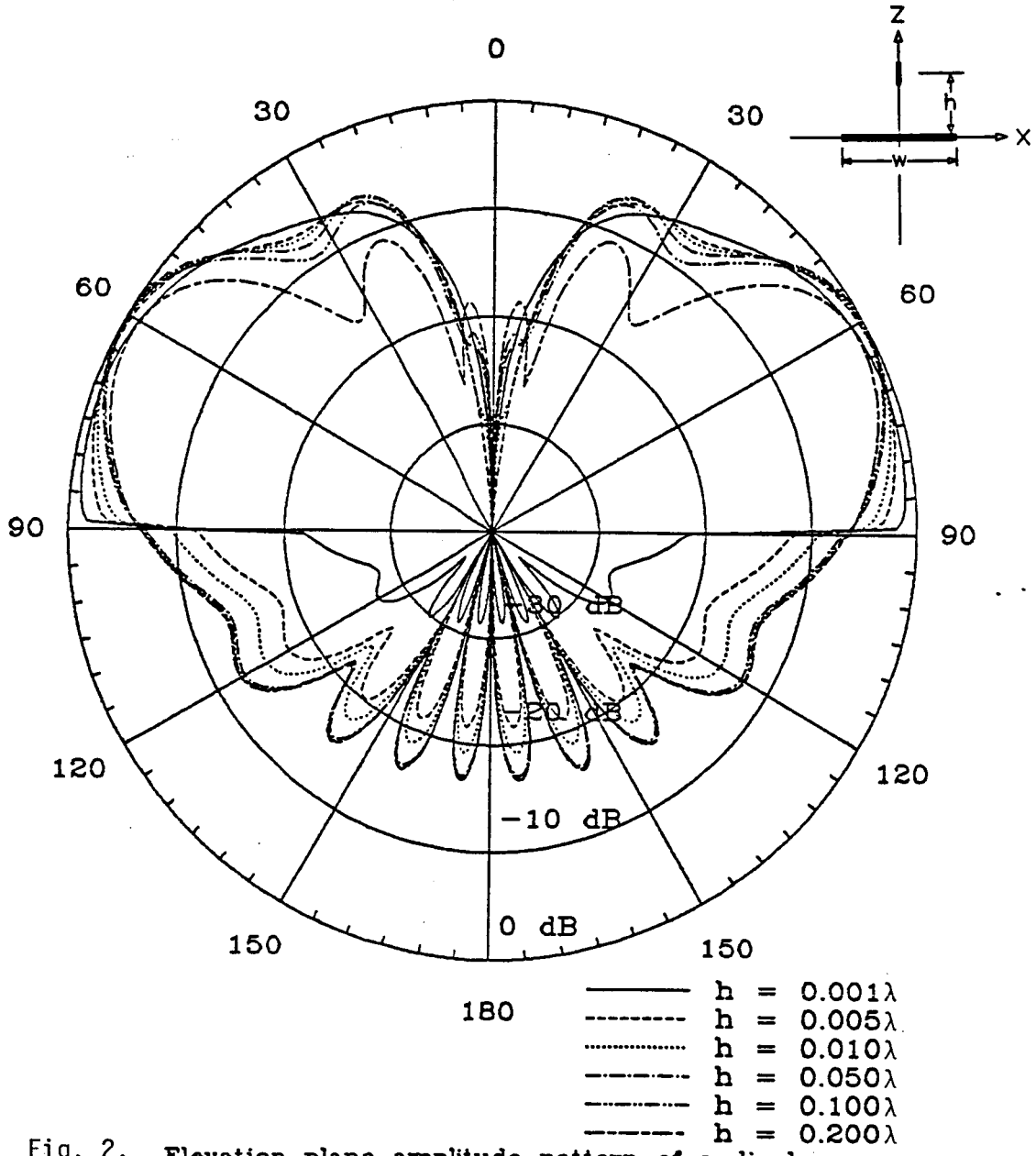

Fig. 2. **Elevation plane amplitude pattern of a dipole above a composite ground plane of width w = 4.064 λ. Vertical dipole at height h. Relative surface impedance η = 0.0016678(1.+j)**

that the diffractions begin to deteriorate at dipole heights h below 0.01 λ. In the limit as $h \to 0$ there would be no diffracted field below the ground plane. The loss of the diffraction mechanisms causes large discontinuities in the total antenna pattern near the incidence and reflection shadow boundaries when $\theta \simeq 90^{\circ}$.

A formulation by Tiberio [7] remedies this situation by achieving a uniform asymptotic solution for the normal incidence case. In [7] the problem of plane wave incidence at the edge of an imperfect conductor wedge, with an observation point P_0 on the $n\pi$ face is considered, and the solution is useful for the present problem of a source on an imperfect conductor by reciprocity. Uniform surface impedance boundary conditions on each face are assumed although the two face impedance are not necessarily the same. The reevaluation of the asymptotic solution is performed since the UTD asymptotic solution vanishes. The more accurate asymptotic solution retains the first nonvanishing term in the expansion of the exact integral representation. The asymptotic solution is uniformly valid at all incidence angles and for all impedance boundary conditions. In addition it provides a smooth transition between the two limiting cases of a hard and a soft perfectly conducting boundary condition.

This formulation is applicable to the present problem which considers the specialized case of a half plane with identical impedances on each side. For the special case of the half plane the difficulty of calculating the Maliuzhinets function $M_2(2\pi, \phi', \theta_0, \theta_2)$ [7, eq. (9)] is considerably reduced. In fact, it can be easily determined in terms of

the Maliuzhinets $\Psi_\pi(\alpha)$ function which is approximated in terms of elementary functions in [5]. For the half plane, [7, eq. (9)] reduces to

$$U^d(p_0) \sim \frac{1}{\sqrt{2\pi k}} \exp(-j\pi/4) \tag{36}$$

$$\cdot \frac{\Psi_\pi(\frac{5\pi}{2} - \phi' + \theta_0)\Psi_\pi(-\frac{\pi}{2} - \theta_0)\Psi_\pi(\phi' + \frac{\pi}{2} + \theta_2)\Psi_\pi(\frac{3\pi}{2} - \theta_2)}{\Psi_\pi(\frac{5\pi}{2} - \phi' - \theta_0)\Psi_\pi(-\frac{\pi}{2} + \theta_0)\Psi_\pi(\phi' + \frac{\pi}{2} - \theta_2)\Psi_\pi(\frac{3\pi}{2} + \theta_2)}$$

$$\cdot \frac{\sin(\frac{\theta_0 - 3\pi}{4})\ \sin(\frac{\theta_2 - \pi}{4})}{\sin(\frac{\theta_0 - \phi'}{4})\ \sin(\frac{\theta_2 + \phi' - 2\pi}{4})}\ \frac{\sin\phi'}{1+\cos\theta_2}$$

$$\cdot \left\{1+\sin\theta_2\left[f_2(\frac{3\pi}{2} - \theta_0) + f_2(\frac{\pi}{2} + \theta_0) + f_2(-\frac{\pi}{2} - \theta_2) + f_2(-\frac{3\pi}{2} + \theta_2) + \frac{1}{2\cos\frac{\phi'}{2}}\right]\right\}$$

$$\cdot \frac{F[2kp\cos^2(\phi'/2)] - F[2kp\sin^2(\theta_2/2)]}{\cos^2(\phi'/2) - \sin^2(\theta_2/2)}\ \frac{e^{-jkp}}{\sqrt{p}}$$

where all parameters are defined in [7] except $\Psi_\pi(\alpha)$ defined in [5]. F[x] is the transition function of the UTD extended analytically for values of x in the complex plane. θ_0 and θ_2 are identical for the half plane problem considered here and are determined by the polarization and surface impedance. The face on which the antenna is mounted is the $\phi=2\pi$ face in this representation.

When this formulation is used for the problem of a vertical current element above the imperfectly conducting finite ground plane, the deterioration of the diffraction coefficients is corrected. Fig. 3 shows the same radiation patterns as Fig. 2 with the use of this surface field diffraction term. The results illustrated show that the edge

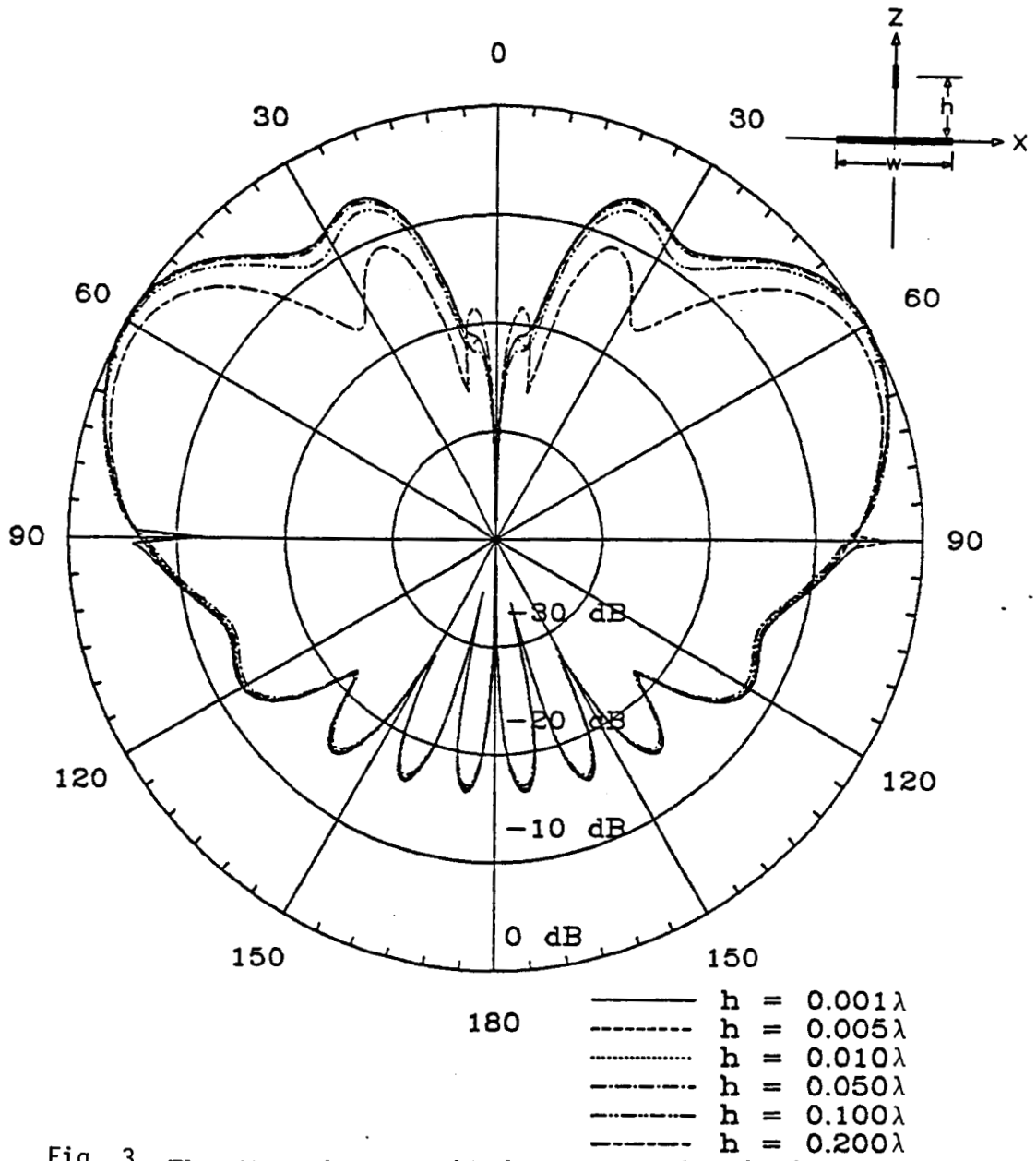

Fig. 3. **Elevation plane amplitude pattern of a dipole above a composite ground plane of width w = 4.064 λ. Vertical dipole at height h. Relative surface impedance η = 0.0016678(1.+j) With surface field correction (Tiberio, et.al. 8/85)**

diffraction exists for an antenna mounted on the surface of an imperfect conductor, and the diffraction provides continuity to the geometrical optics fields. The surface field diffraction guarantees that the solution for the imperfect conductor reduces uniformly to the perfect conductor case.

The pattern of the monopole over the ground plane can be completed using the corrected patterns of Fig. 3. The monopole is subdivided into 10 segments, each with a current proportional to the existing current on the monopole. The resulting pattern is displayed and compared with experimental measurements in Fig. 4. The experimental measurements were reported in [10]. The comparison of the theory with the measured pattern is quite good, and both major and minor lobes are accurately predicted. The measurements are slightly asymmetric, hence the theory may compare better on one side than on the other.

A second contribution mechanism, the surface wave, is currently under study. The surface wave arises from the integral solution of the impedance boundary condition problem when an asymptotic expansion is performed. Conditions for the existence of surface waves has been reported in [11]. If they exist, they are bounded in the angular sector

$$0 < \phi < -\theta_1 - \cos^{-1}\left[1/(\cosh \theta_2)\right] \operatorname{sgn} \theta_2 \tag{37}$$

where ϕ is measured from the illuminated side of the edge and where

$$\theta^s = \theta_1^s - j\theta_2^s = \sin^{-1}(1/\eta) \tag{38a}$$

$$\theta^h = \theta_1^h - j\theta_2^h = \sin^{-1}(\eta) \tag{38b}$$

for the soft and hard polarizations, respectively. The surface waves

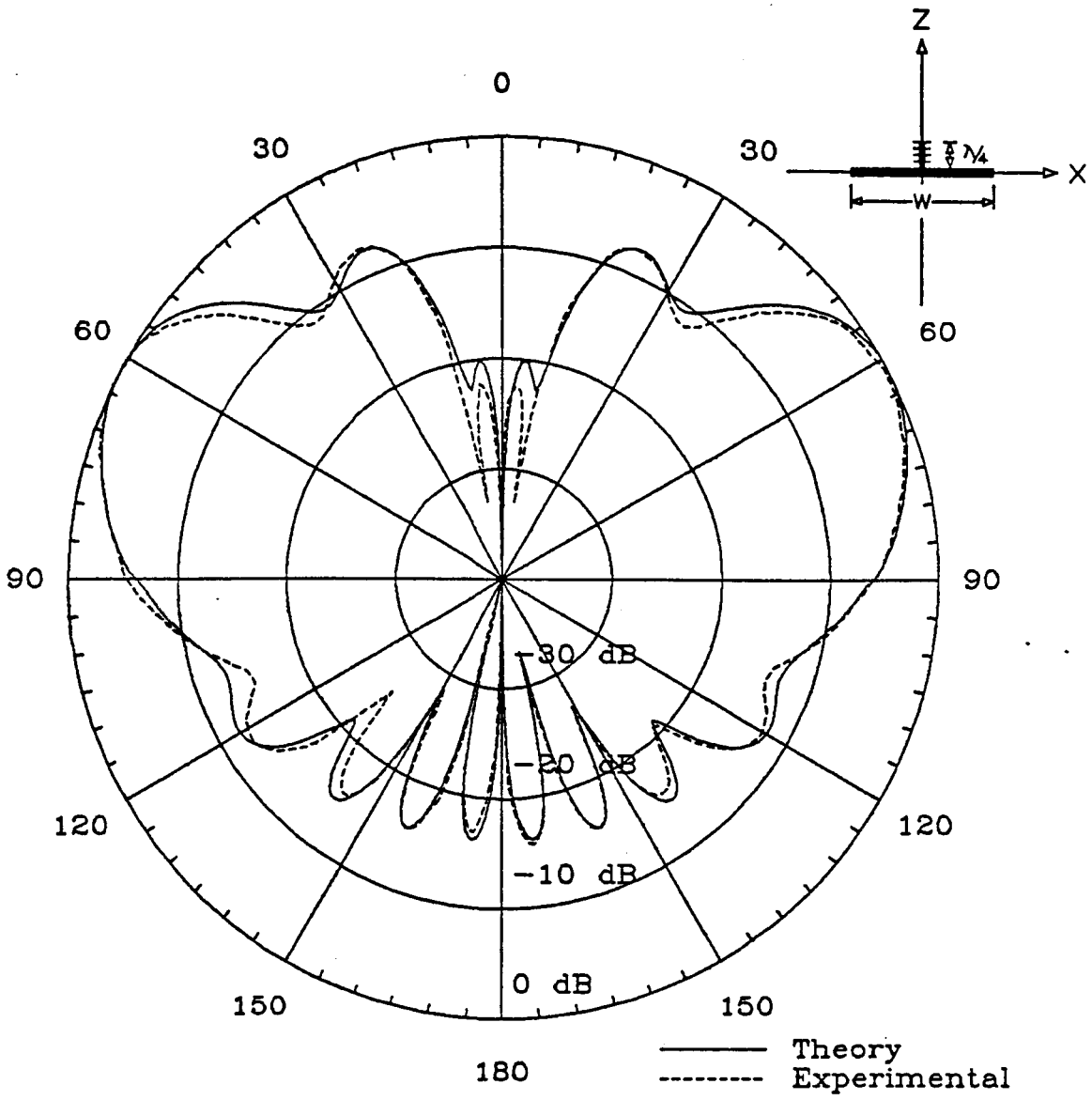

Fig. 4. **Elevation plane amplitude pattern of a λ/4 monopole mounted on a composite ground plane of width 4.064 λ. Relative surface impedance η = 0.0016678(1.+j) Monopole subdivided into 10 infinitesimal elements.**

exist provided [11]

$$\theta_1 + \cos^{-1}\left[1/(\cosh \theta_2)\right] < 0 \qquad (39)$$

For a passive surface $0 \leq \theta_1 \leq \pi/2$, hence if η is real, no surface wave can exist. For capacitive surfaces, only the soft polarized surface wave can exist and for inductive surfaces only the hard polarized surface wave can exist.

IV. COMPUTATIONAL RESULTS

The algorithms of Sections II and III have been used to calculate radiation patterns for a variety of configurations. While the polygonal plate geometry and the antenna pattern can be as complicated as desired, the cases illustrated here involve a simple square plate and a short dipole. The patterns are calculated for three values of normalized surface impedance η=0.001, η=0.25 and η=0.5 where the η=0.001 case is essentially the same as a perfect conductor analysis. The figures show many of the effects expected for a antenna/plate system. These effects include blockage of the antenna pattern by the plate, large grating lobes in the specular reflection region, reduction of the lobing structure as the impedance approaches the free space value, and interference between the direct, reflected and diffracted components.

In Fig. 5, the pattern of a dipole near a square plate is presented. The inset figure in the upper right illustrates the geometry and shows the same orientation represented by the large polar pattern diagram. The square plate lies in the y-z plane and the dipole is parallel to the z axis at a distance of about 6λ from the plate.

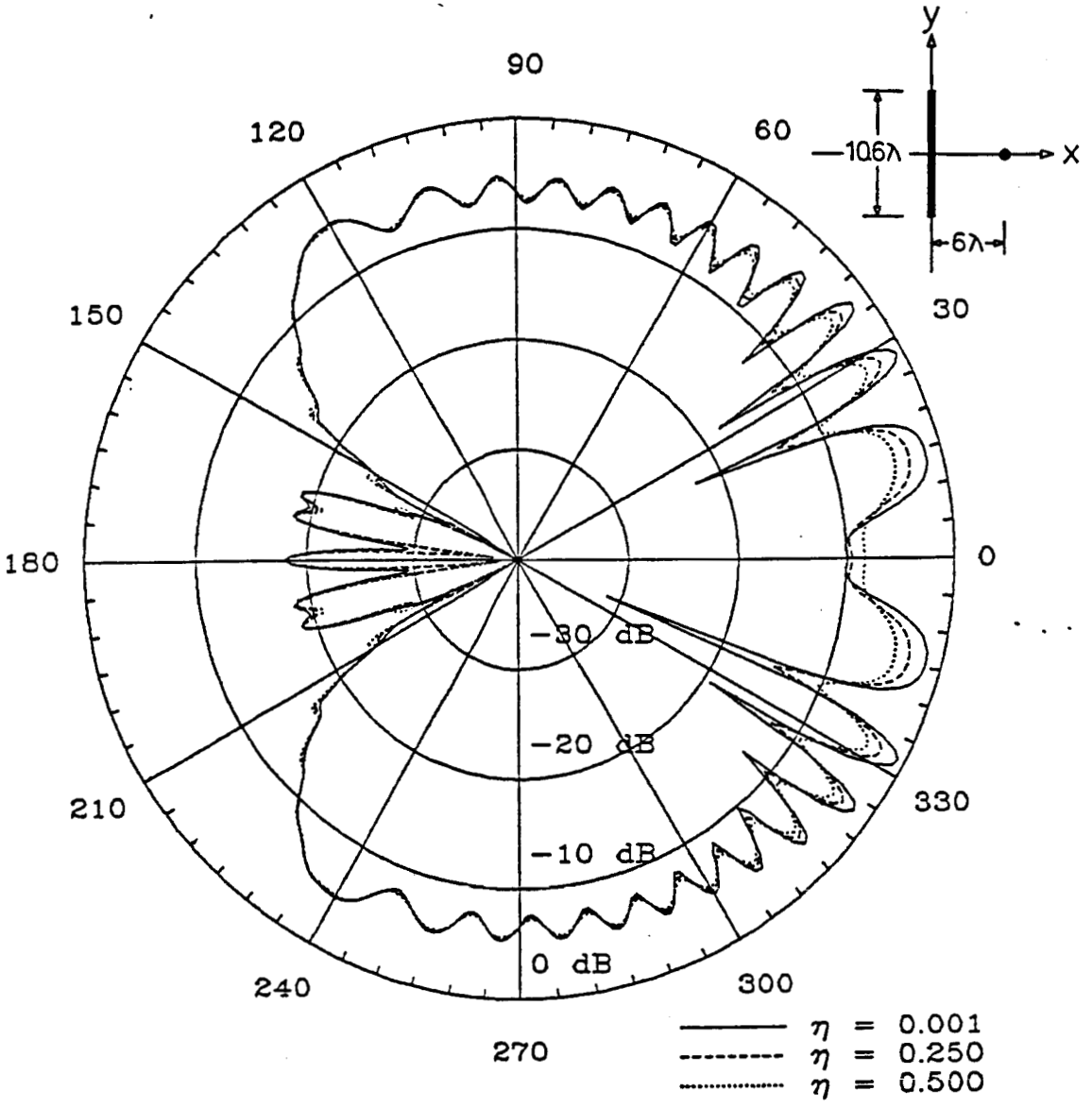

Fig. 5. Amplitude pattern of a dipole near a square plate. Square plate vertices at $(x,y,z)=(0.0,\pm5.2984\lambda,\pm5.2984\lambda)$. Dipole parallel to z axis at $(x,y,z)=(5.9607\lambda,0.0,0.0)$. E_ϕ pattern in x-y plane.

Approximate dimensions are shown in the inset figure while more exact dimensions are given in the lower caption. The pattern shown in the polar diagram represents the E_θ field pattern in the x-y plane, and if the plate were absent the pattern would be a circle, indicative of the isotropic nature of the dipole in the x-y plane. The large grating lobes due to interference of the scattering mechanisms occur on the right side of the plate while blockage of the antenna pattern occurs on the left side of the plate. The lobing structure is diminished as the surface impedance increases toward the free space value.

In Fig. 6, a similar configuration is presented. The dipole is now offset from the center of the plate by 4.9λ. This causes the large grating lobes to move toward the specular direction at around 320°. In addition the pattern blockage due to the plate moves to around 210°.

In Fig. 7, a different pattern cut of the geometry of Fig. 5 is studied. In this figure, the E_θ pattern in the x-z plane is shown. Without the plate the pattern of the dipole would be the classic cut toroid or "figure-eight" shape with nulls at 0° and 180° and lobes at 90° on each side. The large grating lobes again occur on the right side of the plate with blockage occuring behind the plate on the left. The left lobe is largely destroyed. The reduction of the lobing pattern for increased impedance is evident.

In Fig. 8, the inset figure appears to be identical to the inset figure in Fig. 7. The dipole antenna, however, has been lifted off the x-z plane in the y direction to a height of 4.9λ. This is the same configuration as Fig. 6 and places the dipole closer to the edge of the

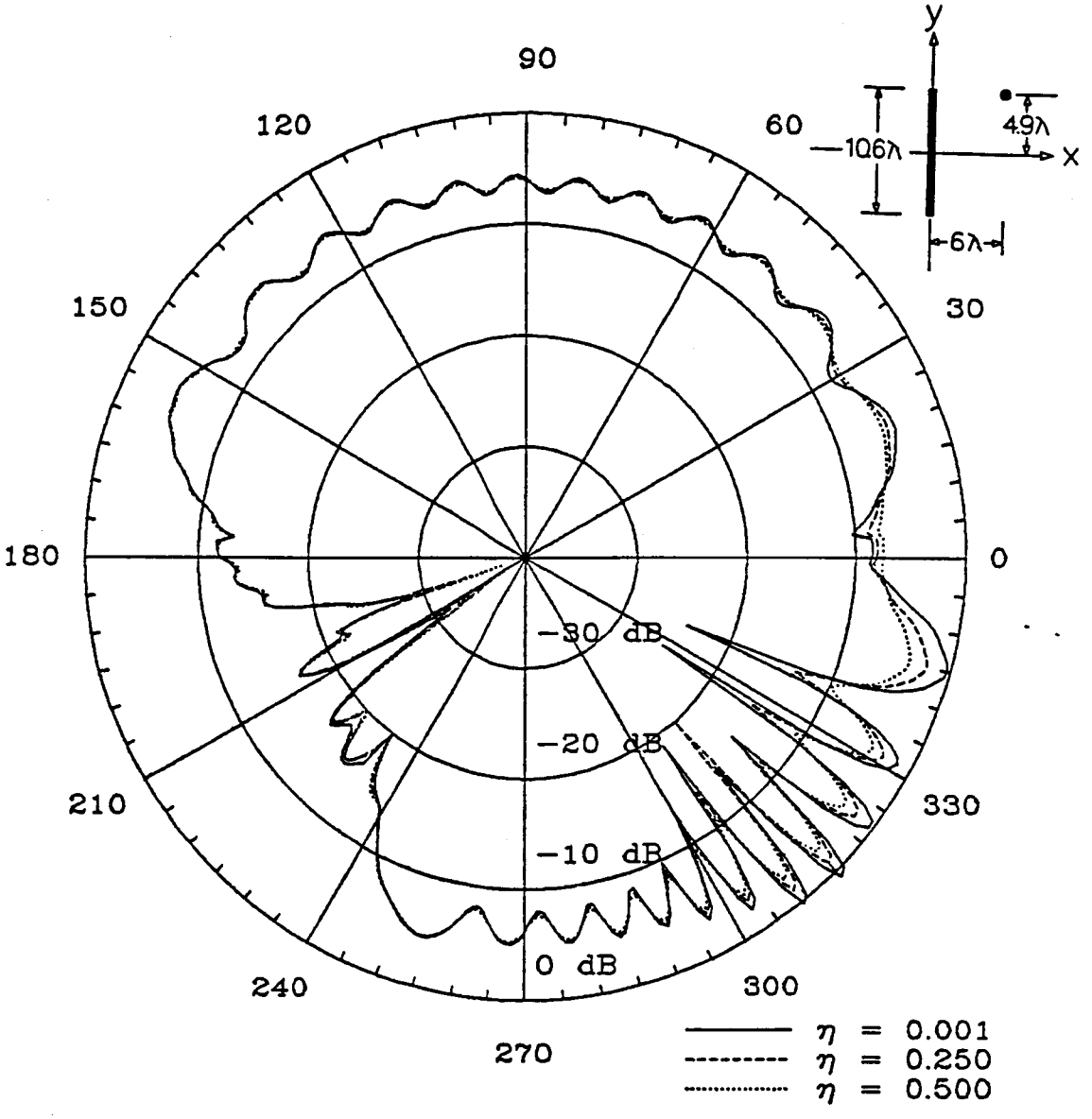

Fig. 6. Amplitude pattern of a dipole near a square plate. Square plate vertices at $(x,y,z)=(0.0,\pm 5.2984\lambda,\pm 5.2984\lambda)$. Dipole parallel to z axis at $(x,y,z)=(5.9607\lambda,4.8569\lambda,0.0)$. E_ϕ pattern in x−y plane.

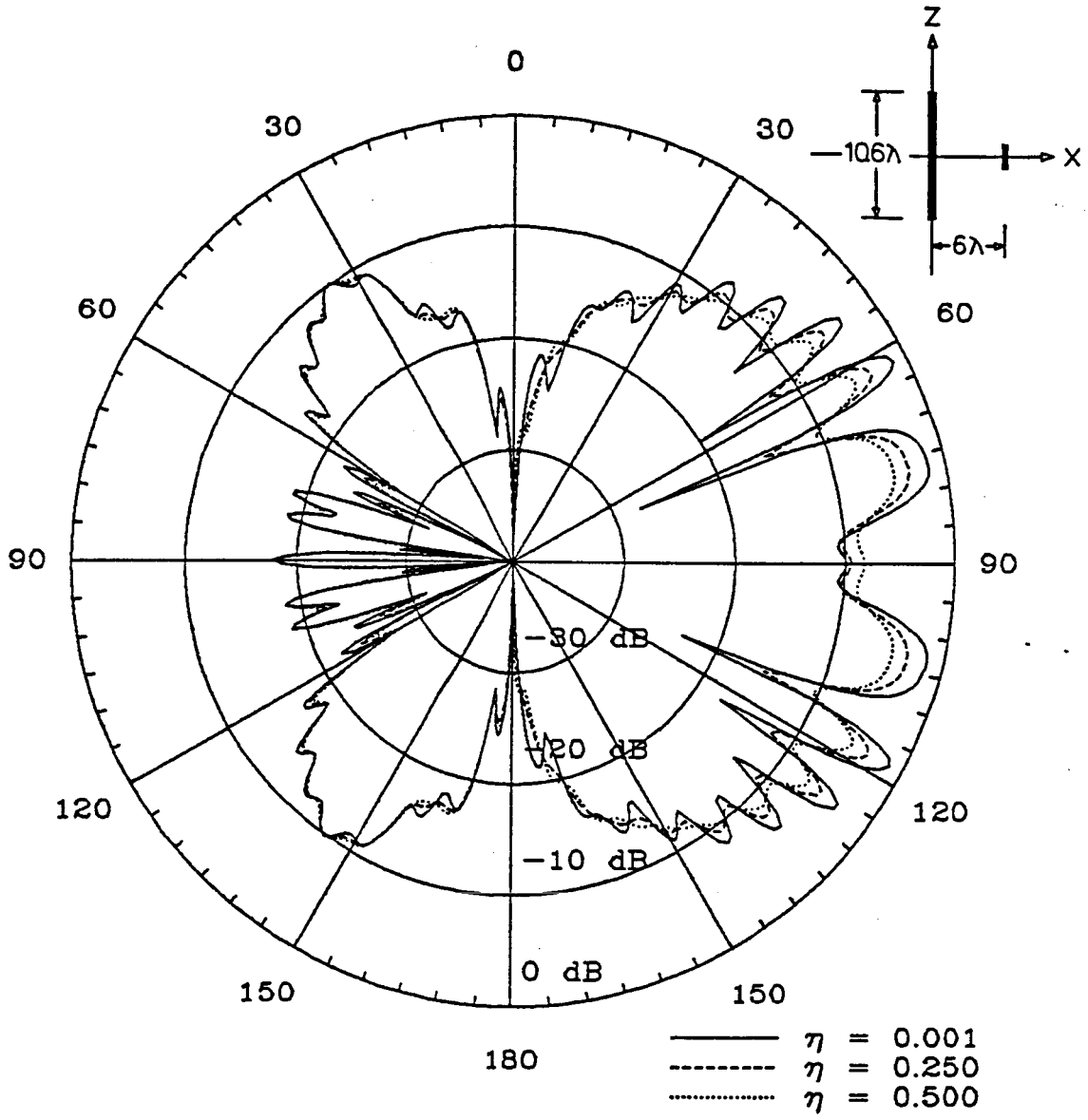

Fig. 7. Amplitude pattern of a dipole near a square plate. Square plate vertices at $(x,y,z)=(0.0,\pm 5.2984\lambda,\pm 5.2984\lambda)$. Dipole parallel to z axis at $(x,y,z)=(5.9607\lambda,0.0,0.0)$. E_ϕ pattern in x–z plane.

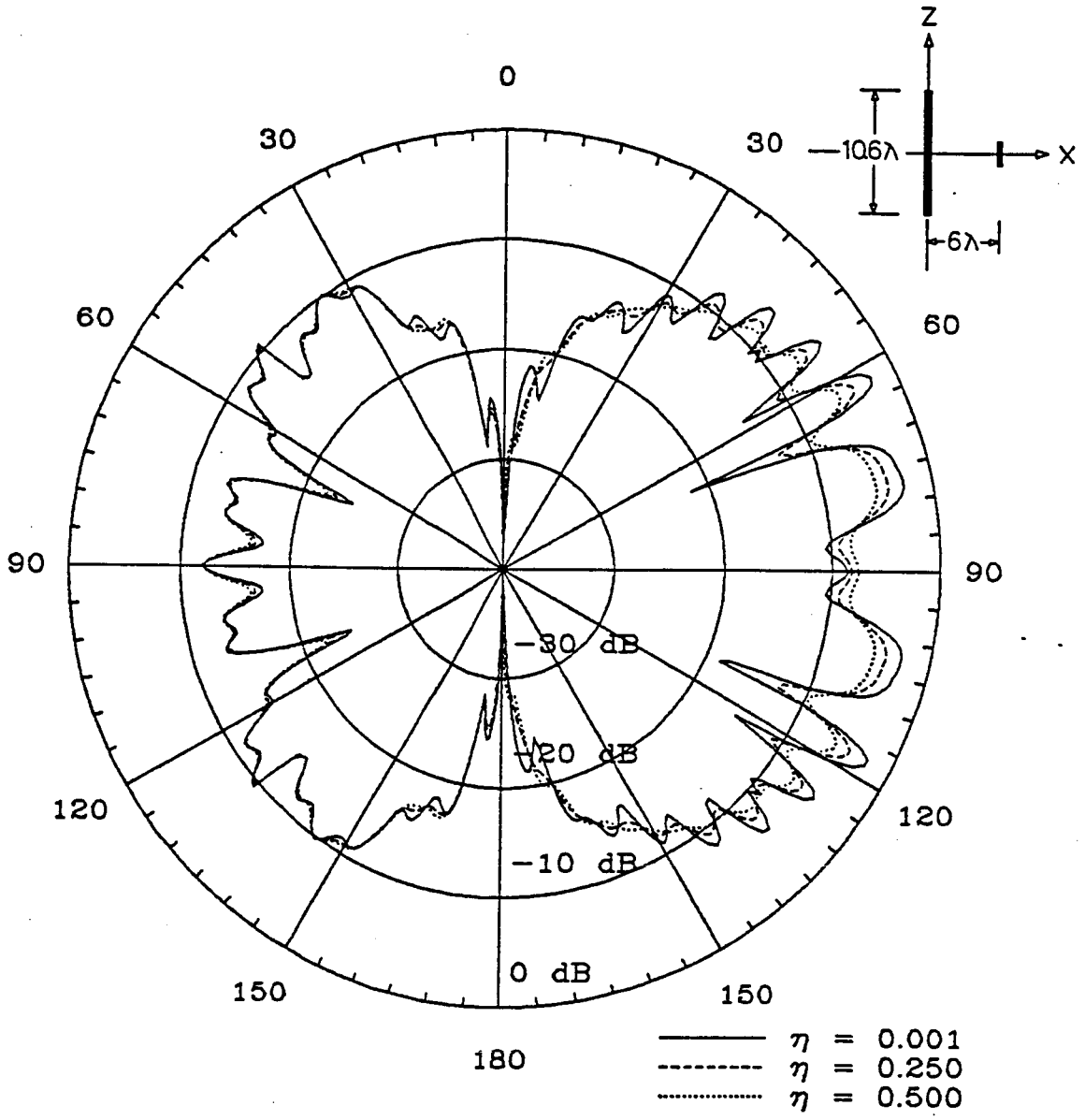

Fig. 8. Amplitude pattern of a dipole near a square plate. Square plate vertices at $(x,y,z)=(0.0,\pm 5.2984\lambda,\pm 5.2984\lambda)$. Dipole parallel to z axis at $(x,y,z)=(5.9607\lambda,4.8569\lambda,0.0)$. E_θ pattern in x−z plane.

plate. This case is of interest because it clearly illustrates discontinuities at 50° and 130° on the left side due to the lack of a corner diffraction component. The diffraction points move as the observation angle is varied and in this case they have moved off the finite edge of the plate. At this time, no corner diffraction coefficients are available for surfaces satisfying the impedance boundary condition and hence these refinements cannot be included. Similar discontinuities are expected whenever a diffraction point migrates off a finite edge.

In Fig. 9, the dipole is aligned along the z axis and the plate is placed in the x-y plane. In this case, the pattern of the dipole in the absence of the plate is the "figure-eight" with nulls at 0° and 180° and major lobes at 90° on each side. In Fig. 10, the dipole is lifted out of the y-z plane and closer to the edge of the plate. The small discontinuities at 140° become apparent on each side due to the migration of the diffraction points off the finite edges. In Fig. 11, the configuration is identical to that shown in Fig. 10 but the pattern is shown in the x-z plane to show the asymmetries.

V. CONCLUSION

During the term of this semiannual progress report, research has been conducted on electromagnetic scattering from impedance structures specifically for antenna pattern calculations. In addition one conference paper was presented and published at an international

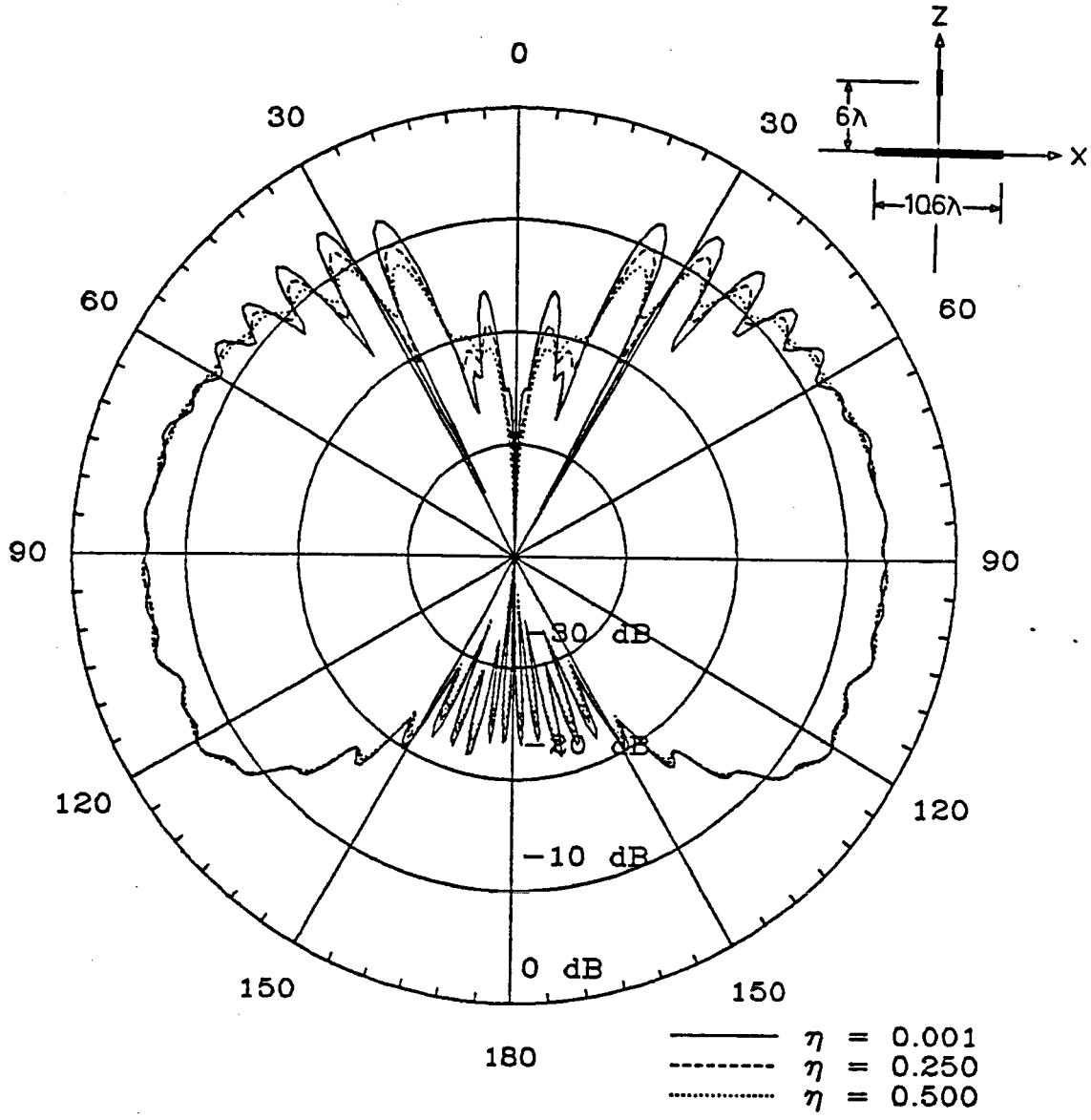

Fig. 9. Amplitude pattern of a dipole near a square plate. Square plate vertices at $(x,y,z)=(\pm 5.2984\lambda,\pm 5.2984\lambda,0.0)$. Dipole parallel to z axis at $(x,y,z)=(0.0,0.0,5.9607\lambda)$. E_θ pattern in x−z plane.

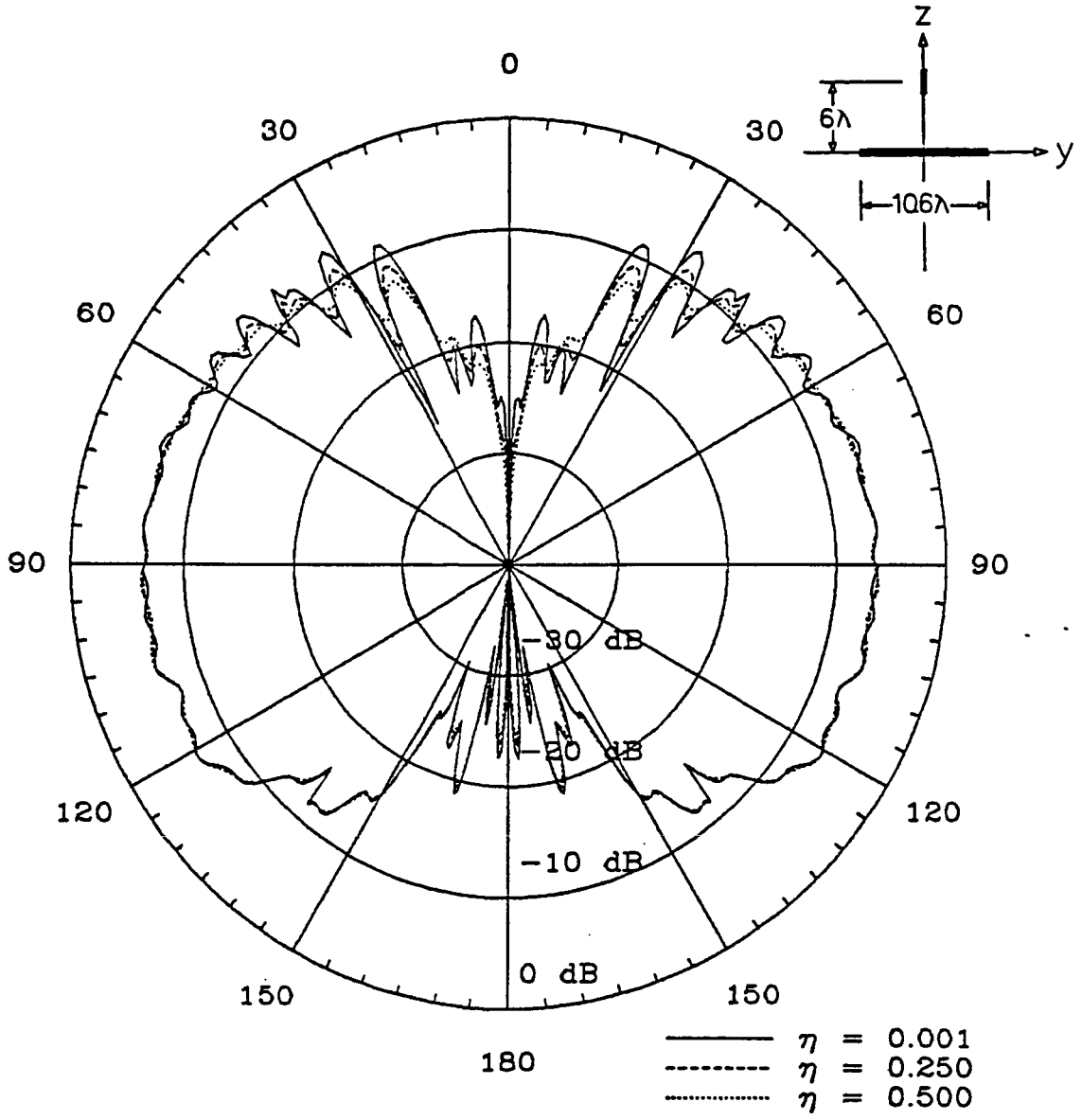

Fig. 10. Amplitude pattern of a dipole near a square plate. Square plate vertices at $(x,y,z)=(\pm 5.2984\lambda, \pm 5.2984\lambda, 0.0)$. Dipole parallel to z axis at $(x,y,z)=(4.8569\lambda, 0.0, 5.9607\lambda)$. E_ϕ pattern in y–z plane.

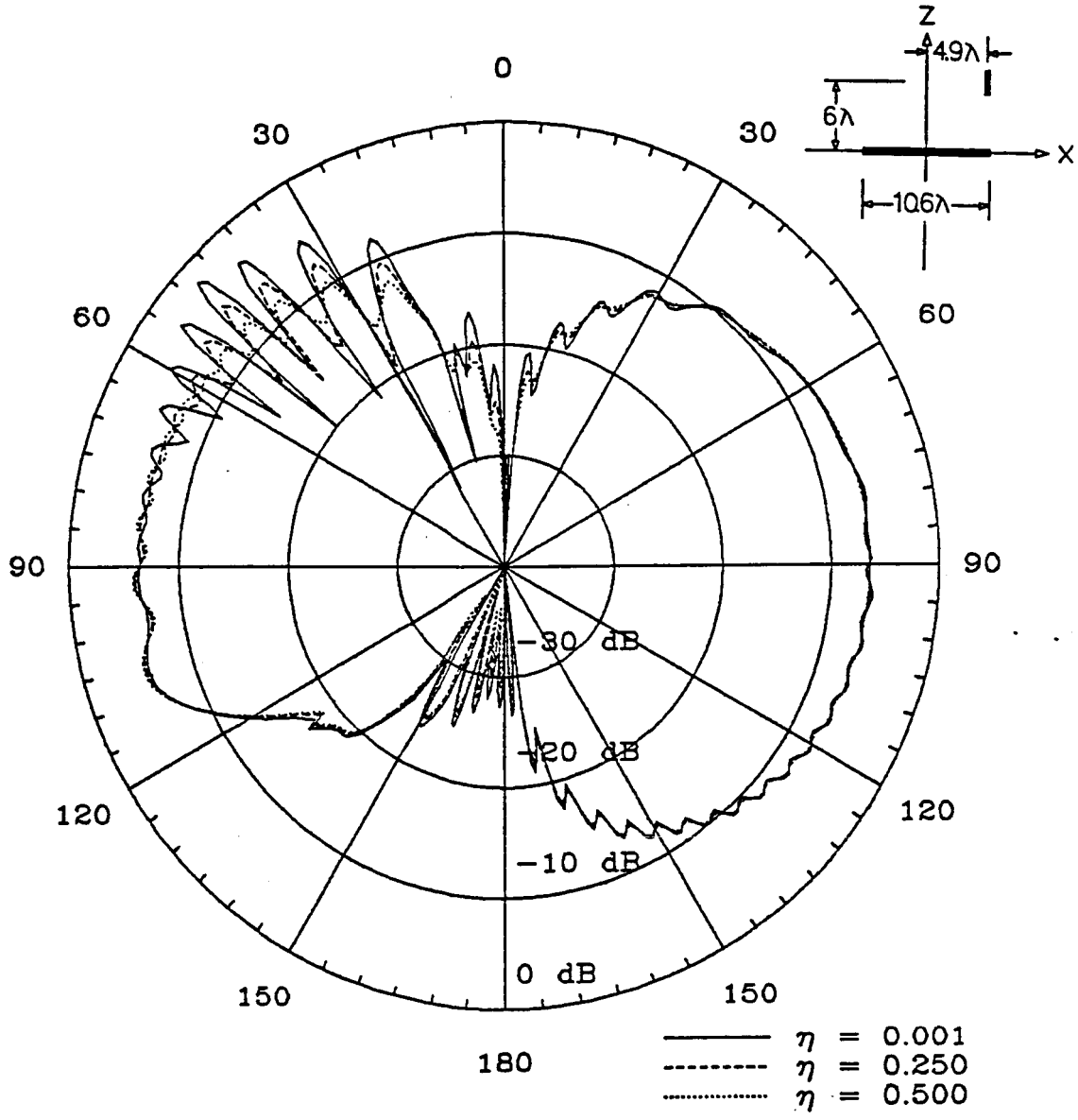

Fig. 11. Amplitude pattern of a dipole near a square plate. Square plate vertices at $(x,y,z)=(\pm 5.2984\lambda, \pm 5.2984\lambda, 0.0)$. Dipole parallel to z axis at $(x,y,z)=(4.8569\lambda, 0.0, 5.9607\lambda)$. E_ϕ pattern in x–z plane.

symposium and two journal papers were accepted and scheduled for publication in the IEEE Transactions on Antennas and Propagation.

The research in electromagnetic scattering involved analysis of reflection and diffraction mechanisms from flat plate structures which satisfied the Leontovich impedance boundary condition. General algorithms were developed for predicting radiation patterns from antennas mounted near plates. The computed patterns show many of the expected characteristics of antenna and plate configurations including the creation of grating lobes, blockage of the antenna pattern by the plate, and reductions in the reflected and diffracted fields with increasing surface impedance.

For antennas mounted directly on flat plates, higher order terms in the asymptotic solution must be considered. Otherwise zero diffracted fields are predicted, which results in large discontinuities in the patterns. The higher order terms provide continuity as well as good agreement with experimental measurement for monopoles mounted on composite ground planes.

Future work in this research will involve introduction of higher order mechanisms to refine the current algorithms. Surface waves, higher order edge diffractions and corner diffractions are example of additional mechanisms which are expected to enhance the predicted patterns. For the surface waves, both launching efficiencies and diffraction mechanisms are topics of study. Further work on the asymptotic expansions for the diffraction coefficients is a topic of interest for predicting scattering when the source is very near, yet not necessarily on, the impedance surface, and also for the oblique

incidence case.

In addition, the theory will be further developed toward calculating backscattering from various structures including plates, disks, and corner reflectors. The reduction of the cross section of the corner reflector by using coated or composite materials is of interest because the dominant backscatter mechanisms is the double reflected field. The double reflected field would be reduced twice because of the double bounce when the corner reflector is an impedance structure rather than a perfectly conducting structure.

REFERENCES

[1] J. L. Volakis, "A uniform geometrical theory of diffraction for an imperfectly conducting half-plane," IEEE Trans. Ant. Prop., vol. AP-34, no. 2, pp. 172-180, Feb. 1986.

[2] R. G. Kouyoumjian and P. H. Pathak, "A uniform geometrical theory of diffraction for an edge in a perfectly conducting surface," Proc. IEEE, vol. 62, no. 11, pp. 1448-1461, Nov. 1974.

[3] T. B. A. Senior, "Diffraction tensors for imperfectly conducting edges," Radio Science, vol. 10, no. 10, pp. 911-919, Oct. 1975.

[4] G. D. Maliuzhinets, "Excitation, reflection and emission of surface waves from a wedge with given face impedances," Soviet Physics, Doklady, vol. 3, pp. 752-755, 1958.

[5] J. L. Volakis and T. B. A. Senior, "Simple expressions for a function occuring in diffraction theory," IEEE Trans. Ant. Prop., vol. AP-33, no. 6, pp. 678-680, June 1985.

[6] R. Tiberio, F. Bessi, G. Manara and G. Pelosi, "Scattering by a strip with two face impedances at edge-on incidence," Radio Science, vol. 17, no. 5, pp. 1199-1210, Sept.-Oct. 1982.

[7] R. Tiberio, G. Pelosi, and G. Manara, "A uniform GTD formulation for the diffraction by a wedge with impedance faces," IEEE Trans. Ant. Prop., vol. AP-33, no. 8, pp. 867-873, Aug. 1985.

[8] R. Tiberio and G. Pelosi, "High-frequency scattering from the edges of impedance discontinuities on a flat plane," IEEE Trans. Ant. Prop., vol. AP-31, no. , pp. 590-596, July 1983.

[9] W. Burnside, "Analysis of on-aircraft antenna patterns," Ph.D. dissertation, Ohio State University, 1972.

[10] C. A. Balanis and D. DeCarlo, "Monopole antenna patterns on finite size composite ground planes," IEEE Trans. Ant. Prop., vol. AP-30, no. 4, pp. 764-768, July 1982.

[11] O. M. Bucci and G. Franceschetti, "Electromagnetic scattering by a half plane with two face impedances," Radio Science, vol. 11, no. 1, pp. 49-59, January 1976.